Progress In Electromagnetics Research C, Vol. 53, 35–43, 2014

Port Isolation Enhancement by Connecting Dual-Element Antenna for MIMO Communications

Wei Ni* **and Yanru Chen**

Abstract—This paper presents a general method to isolate the compact dual-element antenna for mobile radio communications. The basic concept to cancel the coupling current is proposed, and two individual implemental solutions, connecting the transmission lines and the antenna elements, are illustrated respectively. Two examples targeted at 2.4 GHz ISM band have been implemented for the practical cellular phone environment. The antennas are well designed followed by the proposed principle. The result shows that the magnitude of S_{21} between two ports can be no higher than -10 dB in the interested bandwidth after applying the proposed methods. Good agreements are observed between measurements and simulations. It is suitable for application to mobile terminals due to its relatively low profile and good MIMO performance.

1. INTRODUCTION

Multiple input multiple output (MIMO) communication system can substantially improve the spectrum efficiency without increasing extra bandwidth [1]. MIMO system has been adopted in many wireless standards, such as LTE/LTE-A, WiMAX, wireless local area networks (WLAN) etc., and have been considered for future mobile communication systems. Multiple antenna are employed both at base stations and mobile terminals. For base stations, antennas can be separated at several wavelengths. However, the space for mounting multiple antennas on portable terminals is very limited.

Closely-spaced antennas will induce a strong mutual coupling because of the electromagnetic interact among close antenna elements. The impact of mutual coupling on MIMO system performance was intensively studied. On one hand, mutual coupling is a demerit for channel capacity because it greatly degrades the antenna efficiency. On the other hand, mutual coupling can be a merit for the channel capacity because it causes a reduced correlation among antennas which can increase the capacity [2]. Because when antennas come close to each other, the antenna patterns are deformed by electromagnetic scattering; furthermore, the correlation among antenna elements are decreased. At this point, it is better to have the radiation patterns complementary to each other in space in order to receive multipath signals from a variety of directions [3].

For a long time, decoupling among compact antennas has attracted many researchers, and many papers are focused on diminishing the coupling of antennas [15, 16]. In [4], it shows a method to substantially decrease the mutual coupling between elements by replacing the ordinary rectangular microstrip patches in a linear antenna array with fractal patch elements. By etching slots on the ground plane [5, 6], mutual coupling was also suppressed, which can be thought as a bandstop filter between antennas and this effectively reduces current flow between antennas. Similarly, insertion of a ground strip between antennas also shows a good isolation between dual elements [7]. The electromagnetic characteristics of photonic band-gap materials [8] allow reducing the interactions between the antenna and its backward environment. In [9], an optimal power pattern synthesis procedure is able to tackle the mutual coupling and platform effects even for electrically large arrays. A microstrip array

Received 24 June 2014, Accepted 14 August 2014, Scheduled 22 August 2014

* Corresponding author: Wei Ni (wei@jari.cn).

The authors are with the R&D Center, Jiangsu Automation Research Institute, No. 18, Shenghu Rd., Lianyungang 222006, China.

antenna [10] integrated with shapes of 2D-electromagnetic band-gap structure (2D-EBG) shows a low mutual coupling.

In this paper, we propose a general method to achieve high port isolation between two antennas, which is useful for guiding the antenna design targeted in MIMO radio communications. In Section 2, the theory of the proposed method for isolating two antenna elements is presented. Two individual implementation examples follow this theory. And the result of S-parameters, radiation patterns and pattern correlations are shown. In Section 3, the experiment setup for evaluating the MIMO performance of the proposed isolated dual-element antennas is presented. Section 4 gives conclusions.

2. DUAL-ELEMENT ANTENNA CONFIGURATIONS

2.1. Principle Statement

Mutual coupling exists both in transmitting and receiving modes [11]. Here, only transmitting mode is discussed according to the reciprocity principle. The basic concept is illustrated in Figure 1. Suppose that Port #1 is excited and Port #2 is terminated with a 50 Ω load. By connecting a line between two antenna elements, it generates a signal path between two antennas. The current of the artificially added path is probably balanced out by the coupled current of the adjacent antenna if the two currents have the same magnitude and 180 degree phase difference. The subsequent Subsections 2.2 and 2.3 are two different ways to follow this basic principle.

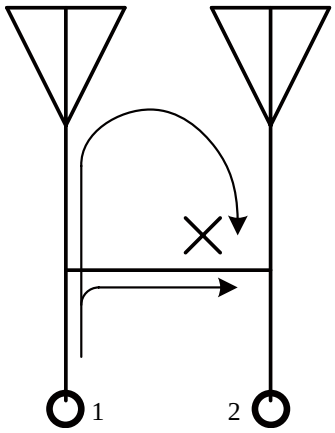

Figure 1. Mutual coupling cancelation in the transmitting mode when two antennas are connected.

2.2. Connecting Transmission Lines

The scheme of the reference antenna (Ant #1) and the proposed dual H-shaped monopole antenna (Ant #2) for enhancing port isolation are given in Figure 2. All the dielectric substrates used here have a 0.8-mm thickness with relative permittivity $\varepsilon_r = 2.2$ and loss tangent $\tan\delta = 0.003$. The ground plane with the size of $25 \times 45\,\text{mm}^2$ is printed on the back surface of the circuit board. The feed point is set up at the end point of 50 Ω transmission line by a 50 Ω SMA coaxial probe. The radiator length is 24 mm (around $\lambda/4$) at 2.4 GHz band. In Figure 2(b), two 50 Ω transmission lines are connected by a straight line and there are two chip inductors ($L = 6.8\,\text{nH}$) are soldered in series in the transmission lines.

For further explaining the decoupling principle, it is assumed that γ is the electrical length of the connection line; Z_0, Z_1, Z_2 are the impedance of input, transmission line (toward the antenna) and the connecting line respectively, thereinto $Z_0 = Z_1 = 50\,\Omega$, as shown in Figure 3.

Generally, the scattering matrix without connection line is:

$$S = \begin{bmatrix} \alpha e^{j\phi} & \beta e^{j\varphi} \\ \beta e^{j\varphi} & \alpha e^{j\phi} \end{bmatrix}. \tag{1}$$

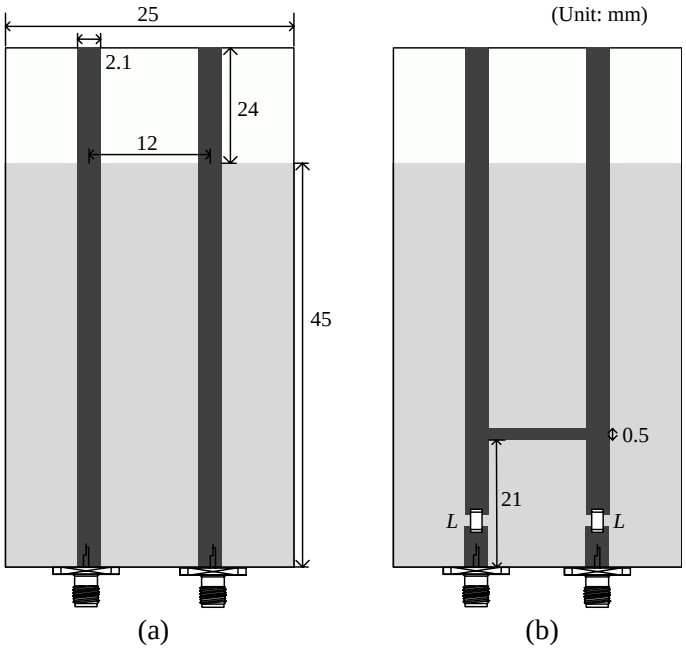

Figure 2. The schematic diagram of the proposed dual-element monopole antenna. (a) Without decoupling (Ant #1). (b) With decoupling (Ant #2).

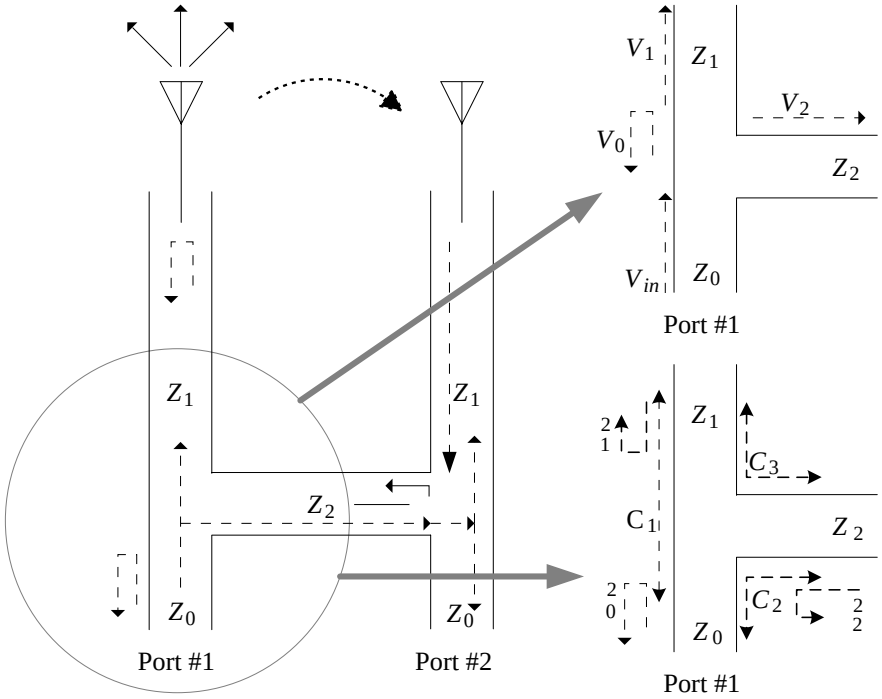

Figure 3. Blocks for decoupling structure by connection two transmission lines when Port #1 is fed.

where α, β are the magnitudes of S_{11} and S_{21}; ϕ, φ are the phases of S_{11} and S_{21}. Here, Port #1 is excited and Port #2 is terminated to a $50\,\Omega$ load.

For symmetry, we only consider that Port #1 is fed. The input voltage V_{in} from Port #1 goes to two branch voltage V_1 (toward the antenna), V_2 (toward the connecting line), and the return voltage

V_0 with corresponding current I_{in}, I_1, I_2 and I_0. The relationship among them is [12]:

$$V_{in} = V_0 + V_1 + V_2 \tag{2}$$
$$I_{in} = I_0 + I_1 + I_2 \tag{3}$$

and the corresponding impedances are:

$$Z_0 = \frac{V_{in}}{I_{in}} = \frac{V_0}{I_0} \tag{4}$$
$$Z_1 = \frac{V_1}{I_1} \tag{5}$$
$$Z_2 = \frac{V_2}{I_2} \tag{6}$$

In the case that Port #1 is fed, the input signal are divided into three branches: reflection (Γ_0), toward the antenna (C_1) and the connecting line (C_2). The power branch coefficients $\Gamma_0^2 (= (\frac{V_0}{V_{in}})^2)$, C_1 $(= \frac{Z_0}{Z_1}(\frac{V_1}{V_{in}})^2)$ and C_2 $(= \frac{Z_0}{Z_2}(\frac{V_2}{V_{in}})^2)$ which flow along path (1) (2) (5) respectively. These three coefficients could be calculated by:

$$\begin{cases} \Gamma_0^2 + C_1 + C_2 = 1; \\ \dfrac{1}{Z_0} = \dfrac{\Gamma_0}{Z_0} + \sqrt{\dfrac{C_1}{Z_0 Z_1}} + \sqrt{\dfrac{C_2}{Z_0 Z_2}}; \\ \Gamma_0 = \dfrac{Z_1 \| Z_2 - Z_0}{Z_1 \| Z_2 + Z_0}. \end{cases} \tag{7}$$

The approximate scattering matrix becomes,

$$S_{11} = S_{22} = \Gamma_0 + C_1 \alpha e^{j\phi} + C_2 \Gamma_1 e^{j2\gamma} \tag{8}$$
$$S_{21} = S_{12} = C_2 e^{j\gamma} + C_1 \beta e^{j\varphi} \tag{9}$$

Based on Eqs. (7) and (9), S_{21} could be minimized by searching Z_2, γ. However, it deteriorates the input impedance matching (S_{11}). Therefore, a matching circuit is necessary for compensating the input matching. In this example, a series inductor with the inductance of 6.8 nH is configured.

In this specific design, the best values of Z_2 and γ are corresponding to the width of connecting line (0.5 mm) and the height apart from the port (21 mm). The simulated S-parameters of Ant #1 and Ant #2 are shown in Figure 4, and the measured ones of Ant #2 are shown in Figure 5 (the result for Ant #1 is omitted for briefness). The simulation results agree with the measured results very well. It is

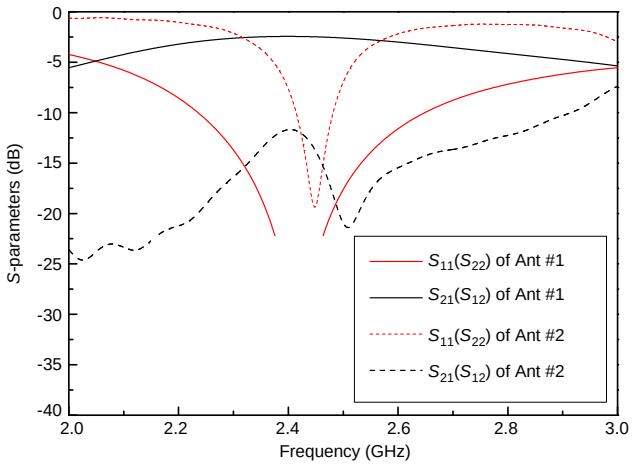

Figure 4. Simulated S-parameters of Ant #1 and Ant #2.

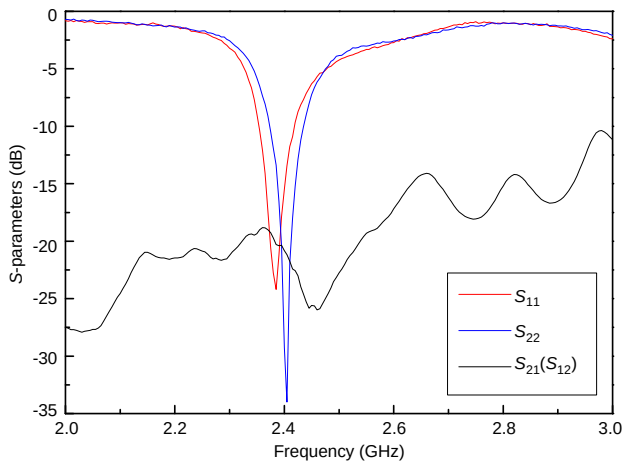

Figure 5. Measured S-parameters of Ant #2.

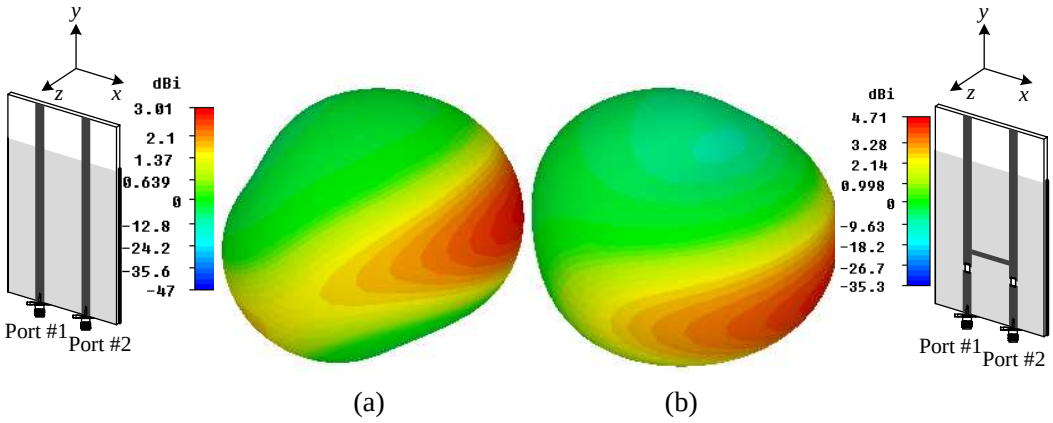

Figure 6. Simulated 3D radiation pattern with Port #1 fed at the frequency of 2.4 GHz. (a) Ant #1. (b) Ant #2.

noticed that the port isolation at 2.4 GHz becomes 20.8 dB, and there is at least 18 dB improvement after the decoupling and matching network is deployed. The isolation improvement is because the coupling wave and the introduced wave are dismissed here and it causes a 18 dB isolation enhancement.

Figure 6 shows the simulated 3D radiation patterns of Ant #1 and Ant #2 at 2.4 GHz, with Port #1 excited and Port #2 terminated to a 50 Ω load. The radiation patterns when Port #2 is fed are not shown here due to the symmetric structure. It is observed that the radiation is toward Port #2, which means the coupling is still very strong although the high port isolation is achieved. Fortunately, it doesn't affect the pattern correlation of two ports. The correlation coefficients ρ_{12} in terms of 3-D radiation patterns can be calculated as [13]

$$\rho_{12} = \frac{E\left\{\left[\sum_{i=1}^{N} F_1\left(\frac{\pi}{2},\phi_i\right)\cdot G_i\right]\left[\sum_{i=1}^{N} F_2\left(\frac{\pi}{2},\phi_i\right)\cdot G_i\right]^*\right\}}{\sqrt{E\left\{\left|\sum_{i=1}^{N} F_1\left(\frac{\pi}{2},\phi_i\right)\cdot G_i\right|^2\right\} E\left\{\left|\sum_{i=1}^{N} F_2\left(\frac{\pi}{2},\phi_i\right)\cdot G_i\right|^2\right\}}}, \tag{10}$$

or,

$$\rho_{12} = \frac{\sum_{i=1}^{N} F_1\left(\frac{\pi}{2},\phi_i\right)\cdot F_2\left(\frac{\pi}{2},\phi_i\right)^*}{\sqrt{\sum_{i=1}^{N}\left|F_1\left(\frac{\pi}{2},\phi_i\right)\right|^2\cdot\sum_{i=1}^{N}\left|F_2\left(\frac{\pi}{2},\phi_i\right)\right|^2}}, \tag{11}$$

where $F_1(\frac{\pi}{2},\phi_i)$ and $F_2(\frac{\pi}{2},\phi_i)$ are the embedded radiation patterns of the two antennas — one antenna is excited while shorting the terminal of the other antenna through its internal impedance; G_i is the Gaussian variable with a zero mean and a unit variance to simulate the multipath fading effect. The correlation between reference antennas and decoupled antennas are 0.438 and 0.182, respectively.

2.3. Connecting Radiators

The scheme of the proposed folded π-shaped antenna (Ant #3) is given in Figure 7. All the dielectric substrates used here have a 1.6-mm thickness with relative permittivity $\varepsilon_r = 4.4$ and loss tangent $\tan\delta = 0.003$. The ground plane with the size of $50 \times 100\,\text{mm}^2$ is printed on the back surface of the circuit board. The feed points are also set up by 50 Ω SMA coaxial probes. The size of π-shaped radiator is $44 \times 7.2\,\text{mm}^2$, which can adhere to the edge of mobile terminals. This design enables a single-element

configuration to act as two individual antennas. The current which flows from one feed point is balanced out with the coupled current of the other radiator. The simulated and measured S-parameters (S_{11}, S_{21} and S_{22}) of the proposed π-shaped antenna are shown in Figure 8 and Figure 9 respectively. A good agreement is observed between the simulation and measurement. The entire frequency band of 2.4–2.5 GHz provides a return loss better than 10 dB. The mutual coupling (S_{21}) between two ports is not larger than -10 dB in the interested band.

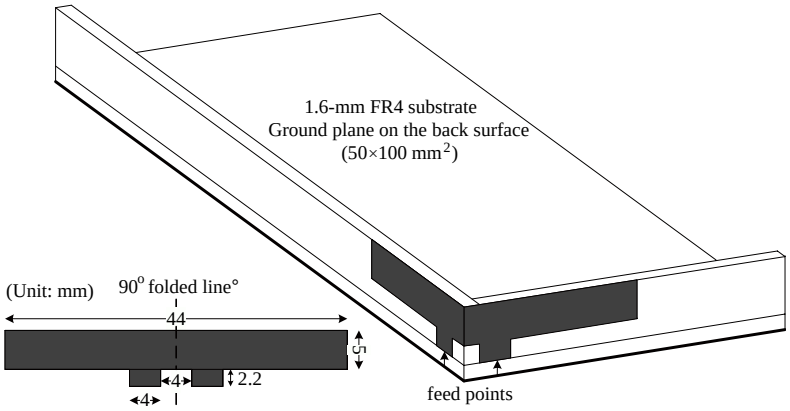

Figure 7. The schematic diagram of the proposed dual-element monopole antenna.

The 3-D radiation patterns were simulated at each of the two ports, with one port excited, while the other was terminated with a 50 Ω matching load. Figure 10 illustrates the simulated 3-D patterns for Port #1 and Port #2 respectively, with the operating frequency of at 2.4 GHz. It is observed that, the peak beams of two ports are directed to different directions, which indicates that a good port isolation can be achieved and the complementary radiation patterns is a benefit when receiving the multipath signals in rich scattering environment. The correlation is 0.117, which is calculated as Equation (11).

3. MIMO PERFORMANCE EVALUATION

3.1. Experimental Setup

The experimental system is designed as a 2×2 MIMO system, which consists of two transmit antennas, two receive antennas, a vector network analyzer, two amplifiers, a PC, a moving controller and a 2-axis moving stage bar as shown in Figure 11. The commercially available sleeve antennas (AT-SL004) [14] are chosen as the transmit antenna. The experiments were conducted in the reverberation room which is approximated to the Rayleigh multipath-rich environment. The dimension of the reverberation chamber is $4 \times 2 \times 2\,\text{mm}^3$. The test of Rayleigh fading channel has been verified via the statistics of the receiving data.

3.2. Experimental Result

It is assumed that the transmitter has no knowledge of the channel, but the receiver knows it perfectly. The transmit power is allocated equally to each transmit antenna. According to Shannon theory, the derivated formula for capacity $\mathcal{C}$ with the assumption that the transmitted signals obey Gaussian distribution independently is expressed as [1]

$$\mathcal{C} = \log_2 \det \left(I_{n_r} + \frac{P}{\sigma^2 n_t} H H^{\dagger} \right), \tag{12}$$

where P is the total transmit power, $(\cdot)^{\dagger}$ for conjugate transpose, H the channel matrix, σ^2 the receiver noise variance, and I_{n_r} identity matrix with size of $n_r \times n_r$. Since in the narrowband radio system, the bandwidth is considered to be narrow enough that the channel response can be regarded as flat over frequency.

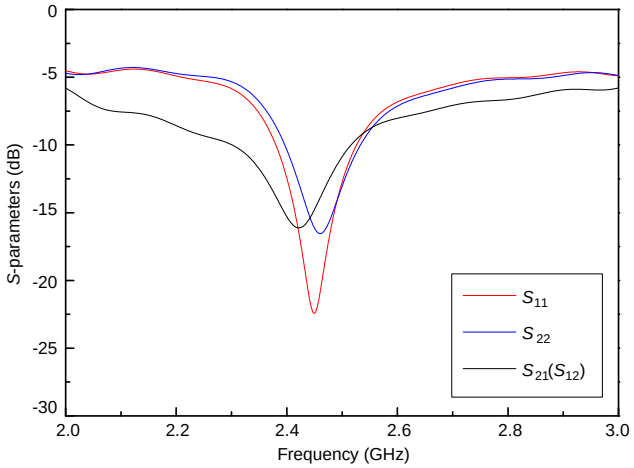

Figure 8. Simulated S-parameters of Ant #3.

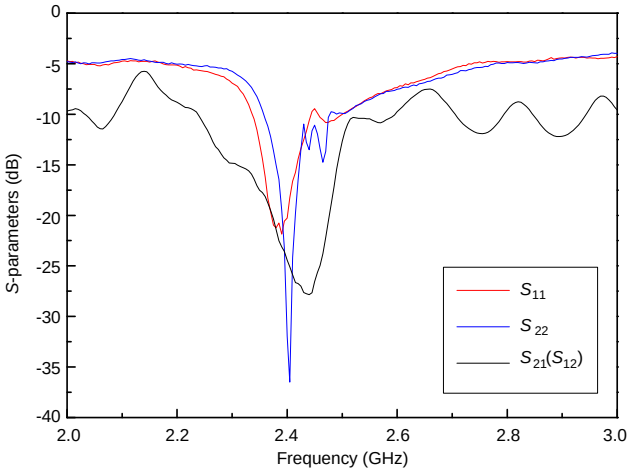

Figure 9. Measured S-parameters of Ant #3.

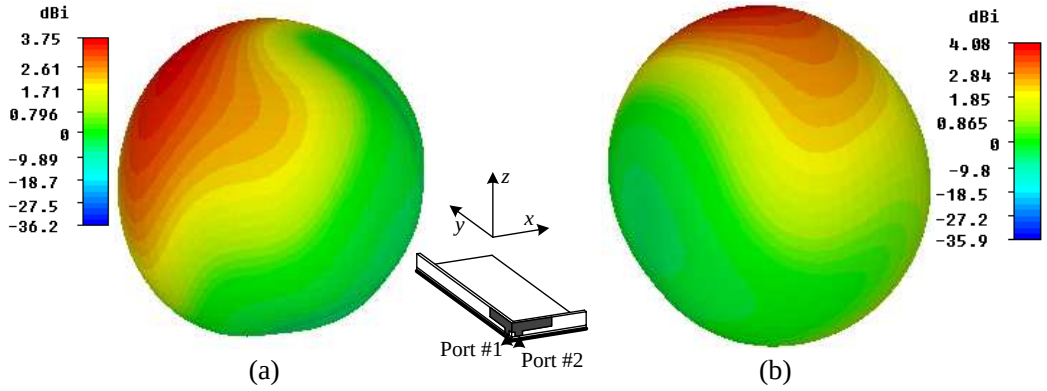

Figure 10. Simulated radiation pattern of Ant #3 at the frequency of 2.4 GHz. (a) Port #1 is fed. (b) Port #2 is fed.

Table 1. Mean SNR (dB), capacity (bps/Hz) and normalized Capacity C_{Nor} for Ant #1, Ant #2 and Ant #3 at 2.4 GHz.

	Mean SNR (dB)	Capacity (bps/Hz)	C_{Nor}
Ant #1	35.72	17.24	82.1%
Ant #2	39.23	22.65	94.38%
Ant #3	39.25	23.16	96.52%

Theoretically, it is assumed that the matrix channel is from Rayleigh channel model, i.e., the real and imaginary part of channel matrix H obey standard normal distribution approximately. 2×2 MIMO Shannon limit curve is also plotted for comparison. The mean SNR, mean capacity C_{mean} and the normalized capacity (C_{Nor}: the ratio of the mean capacity to the predicted value based on independent fading assumptions) are listed in Table 1. It is noticed that the mean capacity of the decoupled antenna is more than that of the reference antenna. The mean SNR of the decoupled antenna is 3.5 dB larger than that of the reference antenna. It is because the reflection efficiency of the decoupled antenna is 3.5 dB larger than that of the reference antenna while the transmitting power is fixed. The decoupled antenna has achieved the higher normalized capacity because it has lower correlation in terms of radiation patterns. All of the aforementioned analysis indicates that the proposed decoupling technique can improve MIMO performance, i.e., channel capacity.

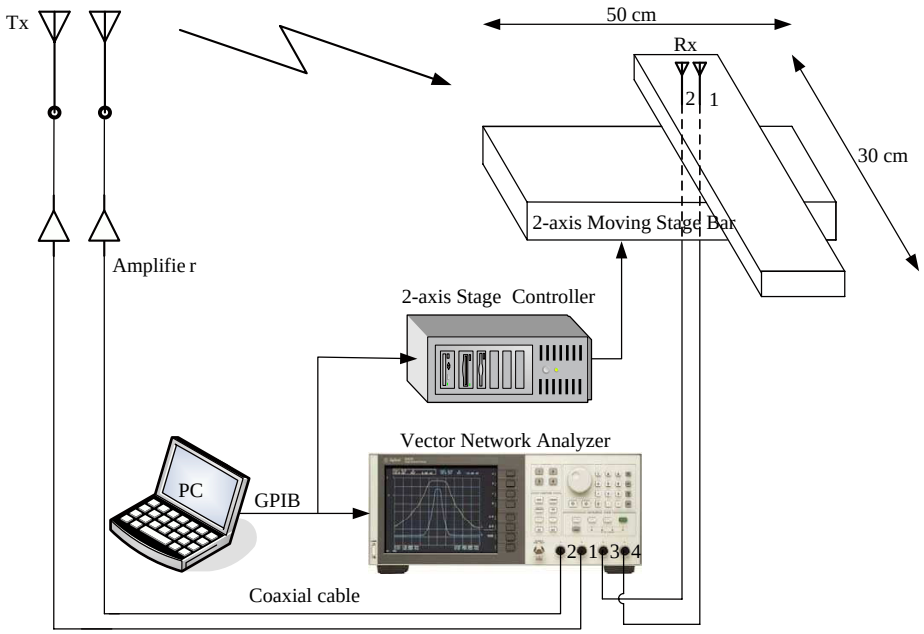

Figure 11. The 2×2 MIMO experimental configuration.

Table 2. The comparison among Ant #1, Ant #2 and Ant #3 in terms of reflection efficiency and pattern correlation at 2.4 GHz.

	reflection efficiency	pattern correlation
Ant #1	43.64%	0.438
Ant #2	97.96%	0.182
Ant #3	98.41%	0.117

3.3. Comparison

The comparison among Ant #1, Ant #2 and Ant #3 in terms of reflection efficiency and pattern correlation at 2.4 GHz is shown in Table 1. The comparison of channel capacity and SNR between reference and decoupled antennas is shown in Table 2. By applying the proposed decoupling techniques, the reflection efficiency is increased by around 3.5 dB. Meanwhile, the correlation is also mitigated due to the deformed radiation patterns. Therefore, both factors can contribute to the enhancement of channel capacity.

4. CONCLUSIONS

A general decoupling method between two adjacent antenna elements has been theoretically and experimentally studied in this research. Two implemental solutions by connecting transmission lines and radiators are proposed, and both ways achieve a good isolation in the required bandwidth. It is demonstrated in experiment that the proposed decoupling techniques can contribute to the enhancement of channel capacity. It can be a guideline for antenna engineers to design MIMO antenna for mobile devices in WiFi/CDMA/LTE standards.

REFERENCES

1. Foschini, G. J. and M. J. Gans, "On limits of wireless communications in a fading environment when using multiple antennas," *Wireless Personal Communications*, Vol. 6, No. 3, 311–335, 1998.

2. Kildal, P. and K. Rosengren, "Correlation and capacity of MIMO systems and mutual coupling, radiation efficiency, and diversity gain of their antennas: Simulations and measurements in a reverberation chamber," *IEEE Communications Magazine*, Vol. 42, No. 12, 102–112, Dec. 2004.
3. Chen, S., Y. Wang, and S. Chung, "A decoupling technique for increasing the port isolation between two strongly coupled antennas," *IEEE Transactions on Antennas and Propagation*, Vol. 56, No. 12, 3650–3658, Dec. 2008.
4. Yousefzadeh, N., C. Ghobadi, and M. Kamyab, "Effect of mutual coupling on capacity of MIMO wireless channels in high snr scenario," *Progress In Electromagnetics Research*, Vol. 66, 41–49, 2006.
5. Chiu, C., C. Cheng, and C. R. Rowell, "Reduction of mutual coupling between closely-packed antenna elements," *IEEE Transactions on Antennas and Propagation*, Vol. 55, No. 6, 1732–1738, Jun. 2007.
6. Sonkki, M. and E. Salonen, "Low mutual coupling between monopole antennas by using two $\lambda/2$ slots," *IEEE Antennas and Wireless Propagation Letters*, Vol. 9, 138–141, 2010.
7. Chou, H. T., H. C. Cheng, H. T. Hsu, and L. R. Kuo, "Investigations of isolation improvement techniques for multiple input multiple output (MIMO) WLAN portable terminal applications," *Progress In Electromagnetics Research*, Vol. 85, 349–366, 2008.
8. Poilasne, G., "Antennas on high impedance ground planes: On the importance of the antenna isolation," *Progress In Electromagnetics Research*, Vol. 41, 237–255, 2003.
9. Bernardi, G., M. Felaco, M. D'Urso, L. Timmoneri, A. Farina, and E. F. Meliado, "A simple strategy to tackle mutual coupling and platform effects in surveillance systems," *Progress In Electromagnetics Research C*, Vol. 20, 1–15, 2011.
10. Nashaat Elsheakh, D. M., M. F. Iskander, E. A. F. Abdallah, H. A. Elsadek, and H. Elhenawy, "Microstrip array antenna with new 2D-electromagnetic band gap structure shapes to reduce harmonics and mutual coupling," *Progress In Electromagnetics Research C*, Vol. 12, 203–213, 2010.
11. Balanis, C. A., *Antenna Theory Analysis and Design*, 3rd Edition, John Wiley & Sons, Ltd., 2005.
12. Pozar, D. M., *Microwave Engineering*, 3rd Edition, University of Massachusetts at Amherst, 2005.
13. Ozdemir, M. K., H. Arslan, and E. Arvas, "On the correlation analysis of antennas in adaptive MIMO systems with 3-D multipath scattering," *Proc. of IEEE Wireless Communication Network Conference*, Vol. 1, 295–299, 2004.
14. TSS-JAPAN Co., Ltd., http://www.tssj.co.jp/antena.htm.
15. Li, G., H. Zhai, Z. Ma, C. Liang, R. Yu, and S. Liu, "Isolation-improved dual-band MIMO antenna array for LTE/WiMAX mobile terminals," *IEEE Antennas and Wireless Propagation Letters*, Vol. 13, 1128–1131, 2014.
16. Shoaib, S., I. Shoaib, N. Shoaib, X. Chen, and C. G. Parini, "Design and performance study of a dual-element multiband printed monopole antenna array for MIMO terminals," *IEEE Antennas and Wireless Propagation Letters*, Vol. 13, 329–332, 2014.